



Published in final edited form as:

*Biomech Model Mechanobiol.* 2018 October ; 17(5): 1281–1295. doi:10.1007/s10237-018-1026-7.

## Compromised Mechanical Homeostasis in Arterial Aging and Associated Cardiovascular Consequences

J. Ferruzzi<sup>1,\*</sup>, D. Madziva<sup>1</sup>, A.W. Caulk<sup>1</sup>, G. Tellides<sup>2,3</sup>, J.D. Humphrey<sup>1,2</sup>

<sup>1</sup>Department of Biomedical Engineering, Yale University, New Haven, CT, USA

<sup>2</sup>Vascular Biology and Therapeutics Program, Yale School of Medicine, New Haven, CT, USA

<sup>3</sup>Department of Surgery, Yale School of Medicine, New Haven, CT, USA

### Abstract

Aging leads to central artery stiffening and associated hemodynamic sequelae. Because healthy arteries exhibit differential geometry, composition, and mechanical behaviors along the central vasculature, we sought to determine whether wall structure and mechanical function differ across five vascular regions – the ascending and descending thoracic aorta, suprarenal and infrarenal abdominal aorta, and common carotid artery – in 20-week versus 100-week old male wild-type mice. Notwithstanding generally consistent changes across these regions, including a marked thickening of the arterial wall, diminished *in vivo* axial stretch, and loss of elastic energy storage capacity, the degree of changes tended to be slightly greater in abdominal than in thoracic or carotid vessels. Likely due to the long half-life of vascular elastin, most mechanical changes in the arterial wall resulted largely from a distributed increase in collagen, including thicker fibers in the media, and localized increases in glycosaminoglycans. Changes within the central arteries associated with significant increases in central pulse pressure and adverse changes in the left ventricle, including increased cardiac mass and decreased diastolic function. Given the similar half-life of vascular elastin in mice and humans but very different life-spans, there are important differences in the aging of central vessels across these species. Nevertheless, the common finding of aberrant matrix remodeling contributing to a compromised mechanical homeostasis suggests that studies of central artery aging in the mouse can provide insight into mechanisms and treatment strategies for the many adverse effects of vascular aging in humans.

### Keywords

arterial stiffness; elastic energy; fibrosis; diastolic function; ventricular hypertrophy

## INTRODUCTION

Aging is a dominant risk factor for many cardiovascular diseases due, in part, to marked changes in central artery geometry, composition, mechanical properties, and function. Such

Address for Correspondence: J.D. Humphrey, Ph.D., Department of Biomedical Engineering, Malone Engineering Center, Yale University, 55 Prospect Street, New Haven, CT, 06520 USA, jay.humphrey@yale.edu.

\*Currently: Department of Biomedical Engineering, Boston University, Boston, MA, USA

**Conflicts of Interest:** None

changes tend to manifest as a structural stiffening of these arteries, which via associated effects on the hemodynamics increases the work load on the heart and increases microvascular damage in end-organs such as the brain and kidneys (Safar 2009; Laurent and Boutouyrie 2015). Among other reasons, aged central arteries dilate and stiffen in humans due to both a mechanical fatigue of medial elastic fibers and an increased deposition or cross-linking of collagen fibers (O'Rourke and Hashimoto 2007). These microstructural changes, in turn, increase carotid-femoral pulse wave velocity and thus central and end-organ pulse pressures (Lakatta et al. 2009). Given the normal gradient in the elastin:collagen ratio along the aorta, there is strong motivation to determine whether aging-induced changes in composition and mechanical properties similarly vary along the central vasculature.

In this paper, we present the first detailed quantification of wall composition and passive biaxial mechanical properties across multiple central arteries as a function of normal aging in wild-type mice. Specifically, *in vitro* biaxial testing was used to assess diverse biomechanical metrics – including wall stress, stiffness, and energy storage – in 20-week and 100-week old male wild-type mice. Despite preserved elastic lamellae, there were qualitatively consistent increases in structural stiffness across the five different segments of central arteries studied, though generally with greater changes in abdominal than thoracic vessels. Importantly, failure to maintain circumferential wall stress and material stiffness at normal levels suggested a compromised mechanical homeostasis (cf. Humphrey, 2008). *In vivo* measurements of central artery hemodynamics and cardiac function further revealed increased peripheral and central pulse pressures, left ventricular hypertrophy, and diastolic dysfunction consistent with many clinical reports.

## METHODS

### In Vivo Measurements.

All animal procedures were approved by the Institutional Animal Care and Use Committee of Yale University. Normal male wild-type mice, obtained as *Fbln5<sup>+/+</sup>* by breeding *Fbln5<sup>+/-</sup>* mice for a study of fibulin-5 deficiency (Ferruzzi et al. 2015), were allowed to age naturally to ~100 weeks. At the prescribed endpoint, tail-cuff blood pressures were recorded using a CODA system (Kent Scientific Corporation, Torrington, CT). Animals were subsequently anesthetized using inhaled isoflurane (2–3% for induction, 1.5% for maintenance) and transferred to an ultrasound platform, with body temperature maintained at 37°C, to collect physiologic information *in vivo*. We employed recently established methods for both measurement and analysis, details of which can be found elsewhere (Ferruzzi et al. 2018). The resulting *in vivo* data included echocardiography and ultrasound, collected using a high-frequency Vevo 2100 system (Visualsonics, Toronto, Canada) and a linear array probe (MS550D, 22–55 MHz), as well as invasive pressures collected using an SPR-1000 catheter (Millar, Houston, TX, USA) with an outer diameter of 1F. The pressure catheter was inserted via a right carotid cut-down and advanced to the middle of the ascending aorta under ultrasound guidance to measure anesthetized central blood pressures. The resulting *in vivo* data included left ventricular systolic and diastolic function, regional diameters from M-Mode images, ascending aortic diameter and length from B-Mode cine loops, and central

hemodynamics including blood velocity from pulsed-wave Doppler and blood pressure from the Millar catheter.

While still under anesthesia, the mice were euthanized using an intraperitoneal injection of Beuthanasia-D (Merck animal Health, Madison, NJ) at 150 mg/kg. One common carotid artery and the aorta from the root to the iliac bifurcation were excised intact and divided into five segments: ascending thoracic aorta (ATA, from the aortic valve to the root of the brachiocephalic trunk), proximal descending thoracic aorta (DTA, from the left subclavian to the third pair of intercostal branches), suprarenal abdominal aorta (SAA, from the last pair of intercostals to the right renal artery), infrarenal abdominal aorta (IAA, from the left renal artery to the iliac bifurcation), and the left common carotid artery (CCA, from the aorta to the carotid bifurcation). Loose perivascular tissue was removed by blunt dissection under a microscope and side branches were ligated with suture to enable in vitro pressurization, as described below. Use of consistent anatomical landmarks yielded arterial segments having unloaded lengths between 3 and 8 mm, depending on the region, thus allowing us to compare lengths between the two age groups.

### **In Vitro Mechanical Testing.**

Biaxial mechanical tests were performed using established methods, details of which can be found elsewhere for both measurement and data analysis (Ferruzzi et al. 2013). Briefly, excised specimens were cannulated on custom glass pipettes, secured using 6–0 silk sutures, and placed within a custom computer-controlled biaxial testing system (Gleason et al. 2004). After equilibration at 37°C for 15 to 30 minutes in a Hank's buffered physiologic solution, specimens were preconditioned using 4 cycles of pressurization from 10 to 140 mmHg at an estimated value of in vivo axial stretch, which is defined by the axial length at which measured axial forces remain nearly constant upon pressurization (Weiszäcker et al. 1983). Outer diameter and axial length were then recorded for each specimen in the absence of external loading. Next, cyclic pressure-diameter ( $P-d$ ) tests were performed at three fixed axial lengths (at and  $\pm 5\%$  of the estimated in vivo stretch) and cyclic axial force-length ( $f-l$ ) tests were performed at four fixed pressures (10, 60, 100, and 140 mmHg). Whereas  $P-d$  tests were carried out consistently between 10 and 140 mmHg,  $f-l$  tests were executed by varying the axial load between 0 g and a region-specific maximum: 4.5 g for the ATA, 3.0 g for the DTA, 2.5 g for SAA and IAA, and 1 g for the CCA (Ferruzzi et al. 2015). After biomechanical testing, arterial rings of consistent width ( $\sim 0.5$ mm) were cut from each vessel and cross-sectional images were captured using a dissection microscope equipped with a CCD camera, both before and after introducing a radial cut to relieve any residual stress. Unloaded wall thickness and opening angles were measured from these images using semi-automated methods (Ferruzzi et al. 2013).

### **Biomechanical Properties.**

For internal consistency, we quantified the passive biaxial data using a validated four-fiber family constitutive model (Ferruzzi et al. 2013, 2015; Bersi et al. 2016, 2017), namely a Holzapfel-type strain energy function defined by

$$W(\mathbf{C}, \mathbf{M}^i) = \frac{c}{2}(I_C - 3) + \sum_{i=1}^4 \frac{c_1^i}{4c_2^i} \left\{ \exp \left[ c_2^i (IV_C^i - 1)^2 \right] - 1 \right\}, \quad (1)$$

where  $c$ ,  $c_1^i$  and  $c_2^i$  are model parameters,  $\mathbf{C} = \mathbf{F}^T \mathbf{F}$  is the right Cauchy-Green tensor,  $\mathbf{F}$  is the deformation gradient tensor, and  $\mathbf{M}^i = (0, \sin \alpha_o^i, \cos \alpha_o^i)$  is a unit vector denoting the orientation of the  $i^{th}$  family of locally parallel fibers, with angle  $\alpha_o^i$  computed relative to the axial ( $z$ ) direction in the intact traction-free reference configuration. One family of fibers is oriented axially ( $\alpha_o^1 = 0$ ), one circumferentially ( $\alpha_o^2 = \pi/2$ ) and two symmetric diagonally ( $\alpha_o^3 = -\alpha_o^4 = \alpha_o$ , a free parameter determined via a best-fit nonlinear regression of the data); these four fiber families are motivated by the microstructure (Ferruzzi et al. 2011), but are also intended to capture phenomenologically any yet unquantified factors such as smooth muscle versus collagen contributions to circumferential behavior or collagen I:III ratios and cross-link densities. That is, like all similar models, equation 1 is microstructurally motivated, not microstructurally based. The resulting passive Cauchy stresses are (Humphrey 2002)

$$\mathbf{t} = -p\mathbf{I} + 2\mathbf{F} \frac{\partial W}{\partial \mathbf{C}} \mathbf{F}^T, \quad (2)$$

where  $p$  is a Lagrange multiplier that enforces isochoric motions; it was calculated by assuming that the radial stress is small in comparison to the in-plane (biaxial) components.

Best-fit values of the 8 model parameters in  $W$  were determined from data sets combined from the seven biaxial testing protocols (3  $P$ - $d$  and 4  $f$ - $l$ , with  $N$  the total number of equilibrium configurations or data points) using a nonlinear least squares minimization of the error  $e$ , where

$$e = \sum_{i=1}^N \left[ \left( \frac{P^{th} - P^{exp}}{\bar{P}^{exp}} \right)_i^2 + \left( \frac{f^{th} - f^{exp}}{\bar{f}^{exp}} \right)_i^2 \right], \quad (3)$$

with  $P$  and  $f$  the distending pressure and total axial force, respectively, with  $th$  and  $exp$  denoting theoretically determined and experimentally measured values, respectively; an overbar represents an average over all data points  $N$  included in the regression. We focused on data obtained during unloading to compute the stored energy that would be available to do work on the blood during elastic recoil (i.e., energy not dissipated during cyclic loading), which thereby captures an important function of a large artery.

The most relevant values of material stiffness are those at in vivo deformations, which change from diastole to systole. We thus used a theory of small deformations superimposed on large to compute material stiffness linearized about a relevant in vivo state, between diastole and systole, namely (Baek et al., 2007)

$$\begin{aligned} \mathcal{E}_{ijkl} = & 2\delta_{ik}F_{iA}^o F_{jB}^o \frac{\partial W}{\partial C_{AB}} + 2\delta_{jk}F_{iA}^o F_{lB}^o \frac{\partial W}{\partial C_{AB}} \\ & + 4F_{iA}^o F_{jB}^o F_{kP}^o F_{lQ}^o \frac{\partial^2 W}{\partial C_{AB} \partial C_{PQ}} \Big|_{\mathbf{C}^o}, \end{aligned} \quad (4)$$

where  $\mathbf{F}^o$  is the deformation gradient associated with mappings from an appropriate (traction-free) reference to a finitely deformed (distended and extended) in vivo configuration, with  $\mathbf{C}^o$  the associated right Cauchy-Green tensor. Such a reference is defined by the measured in vivo axial stretch (inferred as the cross-over point within  $f-l$  data collected at 60, 100, and 140 mmHg; Ferruzzi et al. 2013) and a physiologically relevant pressure. An energy dissipation ratio (EDR) was calculated, as a percent, from the difference between the loading and unloading second Piola-Kirchhoff stress – Green strain curves, following preconditioning, normalized by the energy associated with loading (Ferruzzi et al. 2015). Finally, we combined in vivo information on arterial diameter and length from ultrasound with unloaded dimensions of excised samples and in vitro material properties to estimate the regional biaxial stress and stiffness likely experienced by central arteries under physiologic loads. Detailed methods and assumptions needed to combine in vivo and in vitro biomechanical data can be found elsewhere (Ferruzzi et al. 2018) and yield a transmural pressure  $P_t$  that accounts for the combined action of the intraluminal pressure (which can be measured via a Millar catheter) and perivascular support (which cannot be measured directly, but can be estimated). This, in turn allows calculation of a regional distensibility as

$$D = \frac{id^{sys} - id^{dia}}{id^{dia}(P_t^{sys} - P_t^{dia})}, \quad (5)$$

where  $id$  indicates luminal (or, inner) diameters measured from ultrasound while superscripts  $sys$  and  $dia$  indicate systole and diastole, respectively.

### Histology.

Following in vitro testing, samples were fixed overnight in 4% formalin while unloaded, then stored in 70% ethanol at 4°C until embedding in paraffin and sectioning at 5 μm. For each group, three samples per region (2 groups × 5 regions × 3 samples = 30 total samples) were stained with Verhoeff Van Gieson (VVG) to identify elastic fibers, Masson’s Trichrome (MTC) to identify fibrillar collagen and cell cytoplasm, Movat’s Pentachrome (MOV) to identify intramural glycosaminoglycans, and Picro-Sirius Red (PSR) to delineate collagen fiber size under polarized light (Eberth et al. 2009). Sections from both groups were stained at the same time to reduce processing artifacts and subsequently imaged using an Olympus BX/51 microscope, using both bright- and dark-field imaging at a 400x total magnification. For each sample and stain, we imaged and analyzed 3 to 6 cross-sections to reduce the impact of intra-specimen variability. We employed a previously developed MATLAB interface to identify the area fractions of each load bearing constituent. Details on methods and parameters for the image analysis can be found elsewhere (Bersi et al. 2012, 2016; Ferruzzi et al. 2015). Briefly, we used background subtraction and pixel-based thresholding to classify each pixel within VVG, MTC, and MOV stained sections as elastin,

collagen, cytoplasm, or medial glycosaminoglycans. Similarly, we identified the fraction of thick (red-orange) or thin (yellow-green) birefringent collagen fibers in the media and adventitia of PSR stained sections. Medial and adventitial areas were determined via automated detection of the external elastic lamina in MOV images (Bersi et al. 2017). We have shown previously that MTC staining may lead to an overestimation of collagen area fractions (Ferruzzi et al. 2015). The area fractions for elastin ( $\varphi^e$ ), fibrillar collagen ( $\varphi^c$ ), cytoplasm ( $\varphi^m$ ), and medial glycosaminoglycans ( $\varphi^g$ ) were thus subject to the constraint that  $\varphi^e + \varphi^m + \varphi^c + \varphi^g \cong 1$ . Based on this assumption, the collagen area fraction for each specimen can be calculated based on the other constituents as  $\varphi^c = 1 - \varphi^e + \varphi^m + \varphi^g$ . We found that calculated ( $\varphi_C^c$ ) and measured ( $\varphi_M^c$ ) collagen area fractions for the entire dataset ( $n = 30$ ) related linearly:  $\varphi_C^c = 1.1108 \varphi_M^c - 0.1814$ . The resulting linear relationship was used to consistently calibrate the measured collagen area fractions, which were thereby corrected for overstaining or co-localization of stains within the elastic lamellae.

### Statistics.

Our combined in vivo and in vitro characterization of central artery function was carried out in  $n = 6$  male *Fbln5<sup>+/+</sup>* mice at 100 weeks of age and resulted in groups of 5–6 samples for each of the above measurements in the different regions. Control data from  $n = 5$  male *Fbln5<sup>+/+</sup>* mice at 20 weeks of age were obtained using identical methods and are reported elsewhere (Ferruzzi et al. 2015, 2018). Histological quantifications were conducted on  $n = 3$  animals per age group. Statistical comparisons used two-sided t-tests in the open source Python library SciPy and data were visualized using the plotting library Matplotlib. A value of  $p < 0.05$  was considered significant and denoted by a superscript \*. Possible trends towards significance are similarly denoted by a superscript † for  $p < 0.1$ .

## RESULTS

Figure 1 shows results from cyclic *P-d* and *f-l* tests, collected at individual values of in vivo axial stretch (Table S1), as a function of region (ATA, DTA, SAA, IAA, and CCA) and age (20 and 100 weeks). Normal aging resulted in a slight leftward shift in the pressure-diameter behaviors (top row) as well as a consistent decrease in the axial force needed to maintain the vessels at their estimated in vivo axial stretch during pressurization (middle row). The latter is consistent with the more dramatic, leftward shift in the axial force-stretch behavior (bottom row). Associated biaxial Cauchy stress-stretch results (Figure S1) suggested further that changes in material properties were anisotropic, with diminished axial stretch contributing to the lower values of intramural biaxial stress. The cyclic testing data were fit well by the four-fiber family model (not shown), with mean best-fit values of the parameters (equation 1) listed in Table S2. Calculated Cauchy stress–stretch behaviors revealed qualitatively similar findings across the five regions with aging, each with lower values of biaxial stiffness consistent with the lower biaxial wall stress (Figure 2, top and middle rows). These values of stiffness were calculated directly (equation 4) even though they are depicted as local slopes on the Cauchy stress-strain curves; see Table S1 for specific values calculated at a common pressure of 120 mmHg. Perusal of results in this table reveals similar changes across all 5 regions, though generally to a greater extent in the abdominal vessels. Finally, calculated iso-energetic contours highlighted another effect of the reduced axial extensibility

in aging, namely, lower values of elastic energy storage capability in all regions (Figure 2, bottom row).

Figure 3 shows representative MOV-stained histological images for all five regions, comparing normal (first row) and aged (second row) cross-sections; overall cross-sectional areas were further divided into medial and adventitial contributions (third row). Aging led to an increased unloaded wall area, especially of the media, along the entire length of the aorta. These changes occurred without development of a neointima. Importantly, elastic lamellar structures appeared intact, though with increased intra-lamellar spacing due to aging-associated increases in medial collagen and glycosaminoglycans despite decreases in cytoplasm (i.e., smooth muscle cell area), especially in the ATA and IAA (fourth row). Overall, the greatest change with aging was an increase in collagen content, hence Figure 4 shows normal (first row) and aged (second row) PSR-stained cross-sections imaged under polarized light to visualize the distribution of collagen fiber sizes. Results are shown separately for the media (third row) and the adventitia (fourth row) in order of decreasing fiber diameter: red, orange, yellow, and green. Aged arteries display a higher percentage of larger fibers in the media, especially in abdominal regions (SAA and IAA), but a lower percentage of smaller fibers in the adventitia, especially in the ATA. A full set of representative bright-field histological cross-sections is given in Figure S2, which highlights regional differences in the four major structural constituents, especially a marked increase in fibrillar collagens with preserved elastic fibers.

Noting that cross-sectional area depends on both diameter and wall thickness, Figure 5 shows that unloaded outer diameter measured from fresh, excised samples prior to testing differed little with aging whereas unloaded wall thickness increased in all regions, but especially so in the ascending thoracic aorta (ATA) and both regions of the abdominal aorta (SAA and IAA). The excised specimens that were tested biaxially also tended to be longer in aging, except for the ATA (Table S1). Measurements of blood pressure using the tail-cuff (conscious, resting) method revealed a significant increase in peripheral pulse pressure (i.e., systolic-diastolic blood pressure) with aging, namely  $42 \pm 3$  mmHg in the 100-week old versus  $36 \pm 1$  mmHg in the 20-week old mice (Table S3). Associated ratios of systolic/diastolic pressures were  $107 \pm 6 / 64 \pm 5$  and  $120 \pm 6 / 84 \pm 6$  mmHg, respectively in 100- and 20-weeks old mice, with heart rates of  $731 \pm 18$  and  $692 \pm 19$  bpm. Hence, normal aging of these male wild-type (*Fbln5<sup>+/+</sup>*) mice seems to increase pulse pressure primarily by lowering diastolic blood pressure. Given the absence of overt hypertension, Figure 5 also shows biomechanical stress, material stiffness, and elastic energy storage calculated at individual values of in vivo axial stretch but a common transmural pressure of 120 mmHg. Noting that these comparisons are based on consistent in vitro loading conditions, more physiologically-relevant comparisons are shown in Figure 6.

As seen in Figure 5, biaxial wall stress and material stiffness decreased in all regions due to aging, likely driven by both the decreased axial stretch and increased wall thickness (see Table S1, which reveals increases in thickness of ~29% in the thoracic aorta, 31% in the carotid, and ~42% in the abdominal aorta). The reductions in stress and material stiffness were ~27% on average across all regions, though greatest in abdominal segments. Interestingly, the age-associated increase in wall thickness  $h$  and decrease in circumferential

material stiffness  $\mathcal{E}_{gggg}$  appeared to be self-compensating in the ATA, DTA, and SAA, with the product  $h\mathcal{E}_{gggg}$  (a highly simplified measure of structural stiffness) essentially unchanged from the value in the 20-week old mice (not shown). Surprisingly, this product was lower than normal in the aged IAA and CCA. Dividing this value of structural stiffness by inner radius  $a$  yields a term similar to that found in the highly idealized Moens-Korteweg equation for estimating pulse wave velocity. Note, therefore, that the deformed inner radius calculated at a common transmural pressure of 120 mmHg decreased in all regions with aging (Table S1), with reductions ranging from ~3% in the thoracic (ATA and DTA) to ~7% in the abdominal (SAA and IAA) aorta and a comparable ~8% in the carotid, again recalling that the histology revealed that there was no development of a neointima. The combination of terms  $h\mathcal{E}_{gggg}/a$  yielded values that were 2–7% higher in the aged mice in the ATA, DTA, and SAA but 10–20% lower in the IAA and the CCA. Although provocative, one must be careful not to over-interpret such regional results since it is the multiaxial structural stiffness that dictates the hemodynamics, with axial properties important as well (Demiray 1992).

A primary function of central arteries is to store energy elastically during systole and to use this energy during diastole to work on the blood. There was a consistent loss of energy storage capability in all five regions (Figure 5), with the degree of reduction ranging from ~28% in the thoracic aorta (ATA and DTA) to ~36% in the IAA and CAA and 44% in the SAA. This reduction in energy storage likely resulted, in part, from the reduced in vivo axial stretch, which ranged from 5% (ATA) to 12% (SAA and CCA), but also from the aforementioned decrease in the area fraction of elastin due to the increase in collagen and glycosaminoglycans (Figure 3). The age-associated increase in energy dissipation ratio (EDR, Table S1) was highest in the SAA, and displayed an increasing trend in most regions, especially the ATA (+68%) and CCA (+39%), with the exception of the IAA (which was unexpected, particularly given the significant increase in glycosaminoglycan fraction shown in Figure 3). Increased EDR may result from increased GAGs (Figure 3).

Invasive measurement of blood pressure using a Millar catheter (under anesthesia) complemented findings from tail-cuff measurement of peripheral pressures and revealed a similarly significant increase in central pulse pressure with aging:  $35 \pm 1$  mmHg in the 100-week old mice versus  $30 \pm 1$  mmHg in the 20-week old mice, with systolic/diastolic pressures of  $102 \pm 3/68 \pm 3$  mmHg and  $99 \pm 2/69 \pm 2$  mmHg (Table S4). Associated heart rates under anesthesia were  $555 \pm 16$  bpm in the older mice and  $459 \pm 15$  bpm in the younger mice, which was significantly different. Interestingly, peak blood velocities measured via Doppler ultrasound were  $148 \pm 11$  and  $51 \pm 7$  cm/s in the ATA and IAA of the older mice, respectively, but only  $107 \pm 13$  and  $29 \pm 5$  cm/s in the younger mice, both significantly different (Table S5). The associated pulse transit time – a measure of the speed of wave propagation measured as the delay between the upstroke of blood velocity waveforms in the ATA and IAA (Ferruzzi et al. 2018) – displayed a mild but non-significant decrease in older mice ( $7.7 \pm 2.2$  ms) with respect to the younger mice ( $12.3 \pm 2.4$  ms). Along with data showing a generalized increase in unloaded lengths and decreased in vivo axial stretches (Table S1), the decrease in pulse transit time suggests that pulse wave velocity was increased in aged animals.



B-mode ultrasound measurements of ATA dimensions over a cardiac cycle revealed similar luminal diameters but increased axial lengths due to aging. Associated in vivo cyclic circumferential and axial strains tended to be less due to aging (Figure S3), but these differences did not reach statistical significance. In contrast, M-Mode ultrasound measurements of changes in inner diameter of the ATA suggested a significant reduction in circumferential strain (Figure S4). Notwithstanding inherent limitations of both methods, it appears that circumferential strain decreased in the ATA alone based on comparisons to similar M-mode measurements in the SAA, IAA, and CCA (Figure S4, noting that the DTA could not be imaged due to interference caused by air in the lungs). Importantly, combining in vivo measurements of arterial dimensions with in vitro mechanical findings enabled us to estimate in vivo values of wall stress, material stiffness, elastic energy storage, and distensibility (Figure 6). Albeit for anesthetized conditions (with blood pressure and heart rate depressed), we again found that circumferential properties were largely preserved (top row) while axial properties shifted towards a less extensible behavior (middle row). In vivo energy storage at systole and diastole was generally lower (bottom row), though higher in the ATA perhaps due to the higher in vivo lengths measured from ultrasound (Figure S3) but preserved unloaded lengths measured in vitro (Table S1). Regardless, cyclic energy storage – a measure of the elastic energy stored at systole that can be used during diastole – seemed to be maintained in normal aging under anesthetized conditions (Figure 6, bottom row), suggesting that, despite increased collagen deposition and thickening and lengthening of the arterial wall, somewhat adaptive decreases in material stiffness and wall stress may allow a nearly maintained mechanical function of central arteries under a low workload. Such a finding seems consistent with older individuals managing well in sedentary activities, though not in physical exertion. Indeed, overall distensibility was decreased in all regions, especially in the ATA and SAA.

Echocardiography revealed that, despite an aging-associated significant increase in mean blood velocity in the ATA and IAA, stroke volume and cardiac output increased only modestly (Table 1). There were significant differences in other left ventricular (LV) metrics, however. Aging resulted in a thicker LV wall, an increase in LV mass, and a diminished LV diastolic function (as measured via the ratio  $E/A$ , where  $E$  and  $A$  measure peak LV filling velocity in Early and late - due to Atrial contraction - diastole), all significant at  $p < 0.05$ . That is, the older mice exhibited signs of diastolic dysfunction with preserved ejection fraction under anesthetized conditions. See Table 1 for additional in vivo metrics of cardiac function, noting that adverse effects could be even greater under resting and especially exercise conditions.

Finally, although unexpected and not analyzed in detail, approximately 33% of the DTAs and 50% of the SAAs experienced a grossly visible intramural delamination during biaxial testing (Figure 7) while none of the ATAs, IAAs, or CCAs experienced any visible mechanical damage. Anecdotally, we have tested hundreds of central arteries from many different mouse models and observed such delaminations in only a few: DTAs or SAAs from transforming growth factor receptor 2 disrupted ( $Tgfr2^{fl/fl}$  + Tamoxifen; Ferruzzi et al. 2016), thrombospondin-2 null ( $Tsp2^{-/-}$ ; Bellini et al. 2017), and chronic angiotensin II infused apolipoprotein-E null ( $ApoE^{-/-}$  + AngII; Bersi et al. 2017) among them. In these three cases, delamination was either expected or not surprising given the mutation or

pharmacological treatment. That DTAs and SAAs from aged male mice experienced such delaminations suggests that, despite a compromised mechanical functionality that was partially offset under low workload by adaptive remodeling, aging seems to compromise structural integrity within particular regions of the aorta.

## DISCUSSION

Mice are ideal, in principle, for studying aging-related effects on central arteries. Their lifespan is a mere 2+ years, advances in instrumentation allow careful *in vitro* and *in vivo* quantification of arterial wall mechanics and cardiovascular function, myriad antibodies are available for biological characterization, and, of course, many genetically modified models are available for study. Importantly, genetic profiling has revealed over 1500 transcripts that are differentially expressed between 6-month old (~26 weeks) and 20-month old (~87 weeks) C57BL/6 wild-type mice (Ramos et al., 2014). Amongst the many differences are changes in cell-matrix adhesions that are essential for the cellular mechano-sensing and mechano-regulation of extracellular matrix that endows the arterial wall with much of its mechanical functionality and structural integrity (Wagenseil and Mecham 2009; Humphrey et al. 2014). Such genetic changes are consistent, for example, with observed decreases in elastin:collagen ratios with aging (cf. Fleenor et al. 2010; Wheeler et al. 2015), which were observed herein across all central arteries studied due to increases in collagens and GAGs, not decreases in elastin (Figure 3). Although (immuno)histological studies provide significant insight into compositional changes that result from altered gene expression, biomechanical tests are essential for determining any associated functional consequences (cf. Zhang et al. 2012). That is, the need for detailed biomechanical phenotyping is clear, which must include circumferential and axial properties (Ferruzzi et al. 2013).

Remarkably, there had not been any prior detailed comparison of biaxial wall mechanics across the main central arteries in aging mice. Rather, most prior studies focused on one region and typically used either ring (e.g., Wheeler et al. 2015) or pressure-diameter (e.g., Fleenor et al. 2010) tests. Ring tests do not address what we have found to be essential roles of axial stress and stiffness in arterial mechanics (Humphrey et al. 2009) and pressure-diameter tests at a single axial stretch do not yield information sufficient for rigorous quantification of biaxial mechanical properties (Ferruzzi et al., 2013). Our data (Figures 1, 2, and 5) revealed a marked aging-associated decrease in the preferred (*in vivo*) value of axial stretch in all regions, which in turn had important effects on calculations of wall stress, material stiffness, and energy storage. Clearly, biaxial testing is critical in biomechanical phenotyping.

Our biaxial data revealed marked, though in some cases partially adaptive, aging-related changes in central artery wall mechanics in the normal male mouse. For example, all five regions exhibited a decrease in the intrinsic circumferential material stiffness when evaluated either at a common pressure of 120 mmHg (Figures 2 and 5) or group specific pressures (not shown). These decreases in material stiffness were offset, in part, by a consistent increase in wall thickness that effectively maintained a simple measure of local structural stiffness near normal in the ATA, DTA, and SAA. Such changes may thus be somewhat adaptive, at least from the perspective of influencing global hemodynamics. Although the IAA experienced

the greatest increase in wall thickness (~43%), it also experienced the greatest reduction in material stiffness, thus resulting in a reduced structural stiffness similar to that of the aged CCA. We emphasize, however, that one must consider more complete measures of local structural stiffness, particularly since theoretical studies reveal the importance of axial wall properties on hemodynamics (Demiray 1992). Full fluid-solid interaction simulations will be needed to address fully the effects of regional variations in wall properties on local and global hemodynamics (Cuomo et al., 2017).

Nevertheless, overall it appears that the intramural cells (smooth muscle or fibroblasts) did not control well either the wall stress or material stiffness in any region, but especially in the abdominal aorta. Indeed, if we define perfect mechano-adaptation as preservation of mean wall shear stress and mean circumferential stress, then we should observe inner radius  $a \rightarrow \epsilon^{1/3} a_h$  and wall thickness  $h \rightarrow \gamma \epsilon^{1/3} h_h$ , where  $\epsilon$  denotes a fold-change in volumetric flow and  $\gamma$  denotes a fold-change in blood pressure, with subscript  $h$  denoting a homeostatic value (Humphrey 2008). The statistically significant increase in wall thickness despite nonsignificant changes in blood flow (actually, slight increases in flow with slight decreases in radius) and mean blood pressure (actually, slight decrease in pressure with marked increase in thickness) suggests a compromised mechanical homeostasis, apparently due mainly to the excessive deposition of collagen and accumulation of glycosaminoglycans (Figures 3 and 4). This finding appears to be consistent with the aforementioned transcriptional deficiencies in cell-matrix interactions observed by Rammos et al. (2014). The increased vulnerability of the DTA and SAA to intramural delamination was unexpected, but dramatic. Aging also seems to compromise structural integrity, at least in select portions of the central vasculature. Similarly, the consistent loss of energy storage capability and increase in energy dissipation revealed a diminished mechanical functionality with aging, again particularly in the abdominal aorta.

There are two primary means by which arteries lose their ability to store strain energy upon cyclic loading: (i) loss of elastic fiber integrity, which reduces resilience directly (Ferruzzi et al. 2016), and (ii) increased deposition and/or cross-linking of collagen, which prevents elastic fibers from extending, which reduces resilience indirectly (Bersi et al. 2016). Recalling prior findings that collagen increases significantly in aged central arteries in mice (e.g., Fleenor et al. 2010; Wheeler et al. 2015), our histological data are consistent with the remodeling of collagen dominating changes in mechanical functionality during normal murine aging. Toward this end, it is interesting to compare the present results with prior data for central arteries from 20-week old littermate *Fbln5*<sup>-/-</sup> mice (Ferruzzi et al. 2015). Fibulin-5 deficiency is thought to impair elastic fiber fibrillogenesis, and the arterial phenotype appears as a type of accelerated aging (Wan et al. 2013). Interestingly, Table 2 in Ferruzzi et al. (2015) reveals that, similar to the biomechanical phenotype of normal aging in males described herein (Table S1), fibulin-5 deficiency results in a consistent decrease in deformed inner radius (10–20%), increase in wall thickness (31–47%), decrease in axial stretch (7–19%), decrease in biaxial wall stress (35–50%), and decrease in energy storage (38–61%) across the same five regions (ATA, DTA, SAA, IAA, and CCA). LV diastolic function is similarly compromised in these mutant mice (Le et al. 2014). Hence all general features of normal aging reported herein are seen in the *Fbln5*<sup>-/-</sup> mice, though to somewhat of a greater extent in fibulin-5 deficiency. Interestingly, the fibulin-5 null ATA alone

exhibited a slight increase in circumferential material stiffness, while preserving axial stiffness, and it exhibited the most dramatic reduction in stored energy. Hence, wherein changes tended to be greater in the abdominal than in the thoracic aorta with normal aging, the most proximal thoracic aorta is most affected in the *Fbln5*<sup>-/-</sup> mouse. This finding is consistent with the ATA normally containing the highest elastin:collagen ratio of all central arteries (noting that elastin area fraction was lower in all regions in the aged mice, though statistically so only in the ATA; Figure 3) and loss of fibulin-5 affecting elastogenesis. Importantly, this comparison between normal aging and effects of compromised elastic fibers suggests a potentially important caveat with regard to mouse models of arterial aging, but further that genetic models of compromised elastic fiber integrity can provide additional insight into aging-like changes (cf. Ferruzzi et al. 2016), though not without some concerns due to potentially altered aging in genetically modified models (Pezet 2008; Wan et al. 2014).

The half-life of vascular elastin appears to be 25+ years in mice (Davis 1993; Sherratt 2009), which is of the same order as that in humans (50+ years; Arribas et al. 2006). This value suggests that most elastic fibers remain intact throughout the lifespan of a normal mouse unless otherwise defective, damaged, or degraded due to disease or injury. The histological images in Figure 3 confirm that the primary elastic laminae were largely normal at 100 weeks of age, suggesting that aging was not driven by the mechanical fatigue of elastic fibers seen in humans (cf. O'Rourke and Hashimoto 2007), but rather by increased deposition mainly of collagen but also glycosaminoglycans. It has been reported that aging of normal mice induces significant changes in adventitial collagen (cf. Fleenor et al. 2010), but we found marked increases in medial collagen as well. Whereas the search continues for ways to repair or replace elastic fibers (Zhang et al. 2012; Coquand-Gandit et al. 2017), it may be possible to reverse remodel some of the aberrant age-related changes in collagen via exercise (Lesniewski et al. 2011) or anti-inflammatory treatment (Fleenor et al. 2012), both of which may exploit the high turnover rates of vascular collagen (Rodriguez-Feo et al. 2005). Clearly, altered collagen is similarly important in human aging and may represent a therapeutic target. We must remain mindful, however, of differences between the human and murine vasculatures, and indeed differences across mouse models. Regarding direct comparisons of our findings with those of the Seals group (Fleenor et al. 2010, 2012; Lesniewski et al. 2011), they found much more marked changes in adventitial collagen (in carotids) than we did. It is noted that they used a different mouse model (B6D2F1 versus our C57BL/6 × 129svEv), that their institution is located at a much greater altitude (5,430 feet versus ours at sea level; cf. Boos et al. 2017), and their mice may have a different microbiome. There is need for consideration of diverse conditions when comparing results across laboratories prior to drawing general, definitive conclusions.

Albeit rare, Hutchinson-Guilford (progeria) syndrome results in a severe form of premature aging in humans. Affected individuals tend to die between 8 and 21 years of age (mean of 13) due to progressive arterial occlusions resulting in myocardial infarction or stroke. Transgenic mouse models of progeria reveal, at 9 to 12 months of age, a thickened media in the thoracic aorta and carotid arteries, with increased intra-lamellar distances due, in part, to diffuse accumulation of glycosaminoglycans associated with smooth muscle cell drop-out (Varga et al. 2006; Capell et al. 2008). There are also increases in intramural collagen, with

some thickening of the adventitia, as well as calcification of the wall. Although more modest, the increases in glycosaminoglycan and collagen area fractions reported herein (Figure 3), with associated decreases in elastin and cytoplasmic smooth muscle area fractions, are consistent with both extreme (progeria) and milder (fibulin-5 deficient) models of premature aging. We discussed elsewhere the likely important role of normal medial glycosaminoglycan concentration in facilitating smooth muscle mechano-sensing, but a detrimental role of diffuse increases in reducing mechano-sensing capability (Roccabianca et al. 2014), which also appears to be consistent with the aforementioned age-associated transcriptional changes (Rammos et al. 2014). Perhaps controlling excess glycosaminoglycan production could be another therapeutic target.

That the primary change in blood pressure was an increase in the pulse, not systolic or mean, pressure is important because vascular growth and remodeling appear to be more sensitive to changes in pulse pressure (Lacolley et al. 2009; Eberth et al. 2010). Aging and hypertension (with increased pulse pressure) are often considered together in reviews of central arterial stiffening (Laurent and Boutouyrie 2015; Humphrey et al. 2016). In both aortic banding- (Eberth et al. 2009; Kuang et al. 2013) and chronic angiotensin- (Wu et al. 2014; Bersi et al. 2016) induced hypertension in mice, much of the increase in mural collagen is in the adventitia, with local angiotensin and inflammation playing important roles. Energy storage, that is mechanical functionality, is also markedly reduced in both of these models (Eberth et al. 2011; Bersi et al. 2017). Interestingly, the aforementioned genetic profiling also revealed a significant change in the local angiotensin system in normal murine aging (Rammos et al. 2014). Clearly then, notwithstanding certain caveats, synthesizing data across multiple murine models promises to provide more general insight into collagen remodeling and its effects on central artery stiffening and hemodynamic sequelae, with continued attention needing to focus on the important roles played by both pulse pressure and adventitial inflammation. Indeed, based on a theoretical study (Latorre and Humphrey 2018), it appears that inflammation can further disrupt mechanical homeostasis, perhaps forcing lower targets for stress and stiffness (cf. Figure S1). In particular, given that the media may be immuno-privileged, the role of the inflammation-prone adventitia cannot be forsaken (Wu et al. 2014; Bersi et al. 2016) even though most clinical assessments focus on changes in intimal-medial thickness when assessing central artery stiffness (cf. Davis et al. 2001).

In summary, well-known gross characteristics of central artery aging and hypertension in humans, including progressive increases in luminal diameter, wall thickness, and structural stiffness (Lakatta et al. 2009; Laurent and Boutouyrie 2015), are mimicked only in part via normal aging in mice. Nevertheless, we recommend that such geometric and mechanical changes should be quantified and compared regionally in humans. Moreover, non-standard metrics, including the intrinsic circumferential material stiffness and elastic stored energy capability (e.g., Ferruzzi et al. 2010; Roccabianca et al. 2014), should be measured and their effects on global hemodynamics evaluated (Cuomo et al. 2017). So, too, we should focus more on differential remodeling in the intima/media and adventitia (cf. Bellini et al. 2014; Bersi et al. 2016). Although fibrillar collagens primarily endow the arterial wall with stiffness and strength (noting that collagen I:III ratios and cross-linking are important, and change), increased collagen can limit the distension of the wall that is needed to store energy

elastically in the elastic fibers. Hence, there is also a continuing need to evaluate in aging and hypertension the roles of decreased endothelial cell nitric oxide production (Lakatta et al. 2009), increased inflammation (Wu et al. 2014), and advanced glycation end-products (Bakris et al. 2004), all of which can affect collagen production and its cross-linking. Indeed, direct measurements of age-associated increases in aortic wall properties confirm a correlation between stiffness and collagen cross-linking (Steppan et al. 2014), hence this especially merits increased attention.

In conclusion, chronological aging tends to lead inexorably to structural stiffening of central arteries in humans with associated adverse hemodynamic sequelae. Consequences of aging can be accelerated by multiple connective tissue disorders as well as increased oxidative or mechanical stress, as in chronic inflammatory diseases or hypertension (Nilsson et al. 2013). There is, therefore, a pressing need to understand better the relations among the genetics, mechanobiology, immunobiology, and biomechanics. Finally, given the importance of arterial aging on hemodynamics (O'Rourke and Hashimoto 2007; Safar 2009), and important couplings between large and small vessels (Laurent and Boutouyrie 2015), there is a pressing need for computational studies that can elucidate effects of regional differences in mechanical properties (Cuomo et al. 2017). The present study provides some of the information that is needed for such studies, with the particular advantage of its derivation from a murine model that exhibits increased structural stiffening of central arteries without overt hypertension and yet presents with increased central pulse pressures and diastolic dysfunction with a preserved ejection fraction.

## Supplementary Material

Refer to Web version on PubMed Central for supplementary material.

## ACKNOWLEDGMENTS

This work was supported, in part, by grants from the National Institutes of Health (R01 HL105297 and P01 HL134605). We thank Nikki Mikush (Staff, Yale School of Medicine) who acquired the ultrasound data and Thomas Stockdale (Visiting Student, University of Cambridge School of Clinical Medicine) who contributed to the early ultrasound analysis.

## REFERENCES

- Arribas SM, Hinek A, Gonzalez MC (2006) Elastic fibres and vascular structure in hypertension. *Pharmacol Therapeutic* 111: 771–791.
- Baek S, Gleason RL, Rajagopal KR, Humphrey JD (2007) Theory of small on large: Potential utility in computations of fluid-solid interactions in arteries. *Comp Meth Applied Mech Engr* 196: 3070–3078.
- Bakris GL, Bank AJ, Kass DA, Neutel JM, Preston RA, Oparil S (2004) Advanced glycation end-product cross-link breakers. A novel approach to cardiovascular pathologies related to the aging process. *Am J Hyperten* 17: 23S–30S.
- Bellini C, Ferruzzi J, Roccabianca S, Di Martino ES, Humphrey JD (2014) A microstructurally motivated model of arterial wall mechanics with mechanobiological implications. *Annl Biomed Engr* 42: 488–502.
- Bellini C, Kristofik NJ, Bersi MR, Kyriakides TR, Humphrey JD (2017) A hidden structural vulnerability in the thrombospondin-2 deficient aorta increases the propensity to intramural delamination. *J Mech Behav Biomed Mater* 71: 397–406. [PubMed: 28412645]

- Bersi MR, Collins MJ, Wilson E, Humphrey JD (2012) Disparate changes in the mechanical properties of murine carotid arteries and aorta in response to chronic infusion of angiotensin-II. *Int. J. Adv. Eng. Sci. Appl. Math* 4: 228–240.
- Bersi MR, Bellini C, Wu J, Harrison DG, Humphrey JD (2016) Excessive adventitial remodeling leads to maladaptive aortic function in angiotensin-induced hypertension. *Hypertension* 67: 890–896. [PubMed: 27001298]
- Bersi MR, Khosravi R, Wujciak AJ, Harrison DG, Humphrey JD (2017) Differential cell-matrix mechanoadaptations and inflammation drive regional propensities to aortic fibrosis, aneurysm or dissection in hypertension. *J R Soc Interface* 14: 20170327. [PubMed: 29118111]
- Boos CJ, Vincent E, Mellor A, Woods DR, New C, Cruttenden R, Barlow M, Cooke M, Deighton K, Scott P, Clarke S, O'Hara J (2017) The effect of high altitude on central blood pressure and arterial stiffness. *J Hum Hyperten* 31: 715–719.
- Capell BC, Olive M, Erdos MR, ... Collins F (2008) A farnesyltransferase inhibitor prevents both the onset and late progression of cardiovascular disease in a progeria mouse model. *PNAS* 105: 15902–15907. [PubMed: 18838683]
- Coquand-Gandit M, Jacob MP, Fhayli W, ... (2017) Chronic treatment with Minoxidil induces elastic fiber neosynthesis and functional improvement in the aorta of aged mice. *Rejuven Res* 20: 218–230.
- Cuomo F, Roccabianca S, Dillon-Murphy D, Xiao N, Humphrey JD, Figueroa CA (2017) Effects of age-associated regional changes in aortic stiffness on human hemodynamics revealed by computational modeling. *PLoS One* 12: e0173177. [PubMed: 28253335]
- Davis EC (1993) Stability of elastin in the developing mouse aorta: a quantitative radioautographic study. *Histochemistry* 100: 17–26. [PubMed: 8226106]
- Davis PH, Dawson JD, Riley WA, Lauer RM (2001) Carotid intimal-medial thickness is related to cardiovascular risk factors measured from childhood through middle age. *Circulation* 104: 2815–2819. [PubMed: 11733400]
- Demiray H (1992) Wave propagation through a viscous fluid contained in a prestressed thin elastic tube. *Int J Engr Sci* 30: 1607–1620.
- Eberth JF, Gresham VC, Reddy AK, Popovic N, Wilson E, Humphrey JD (2009) Importance of pulsatility in hypertensive carotid artery growth and remodeling. *J Hyperten* 27: 2010–2021.
- Eberth JF, Popovic N, Gresham V, Wilson E, Humphrey JD (2010) Time course of carotid artery growth and remodeling in response to altered pulsatility. *Am J Physiol* 299: H1875–1883.
- Eberth JF, Cardamone L, Humphrey JD (2011) Evolving biaxial mechanical properties of mouse carotid arteries in hypertension. *J Biomech* 44: 2532–2537. [PubMed: 21851943]
- Ferruzzi J, Collins MJ, Yeh AT, Humphrey JD (2011a) Mechanical assessment of elastin integrity in fibrillin-1-deficient carotid arteries: implications for Marfan syndrome. *Cardiovasc Res* 92: 287–295. [PubMed: 21730037]
- Ferruzzi J, Vorp DA, Humphrey JD (2011b) On constitutive descriptors of the biaxial mechanical behavior of human abdominal aorta and aneurysms. *J R Soc Interface* 8: 435–450. [PubMed: 20659928]
- Ferruzzi J, Bersi MR, Humphrey JD (2013) Biomechanical phenotyping of central arteries in health and disease: Advantages of and methods for murine models. *Annl Biomed Engr* 41: 1311–1130.
- Ferruzzi J, Bersi MR, Uman S, Yanagisawa H, Humphrey JD (2015) Decreased energy storage, not increased material stiffness, characterizes central artery dysfunction in fibulin-5 deficiency independent of sex. *J Biomech Engr* 137: 0310071–03100714.
- Ferruzzi J, Bersi MR, Mecham RP, Ramirez F, Yanagisawa H, Tellides G, Humphrey JD (2016a) Loss of elastic fiber integrity compromises common carotid function: Implications for vascular aging. *Artery Research* 14: 41–52. [PubMed: 27570569]
- Ferruzzi J, Murtada S-I, Li G, Jiao Y, Uman S, Ting MY, Tellides G, Humphrey JD (2016) Pharmacologically improved contractility protects against aortic dissection in mice with disrupted transforming growth factor-beta signaling despite compromised extracellular matrix properties. *ATVB* 36: 919–927.

- Ferruzzi J, Di Achille P, Mikush N, Sinusas AJ, Tellides G, Humphrey JD (2018) Combining in vivo and in vitro biomechanical data reveals key roles of perivascular tethering and axial motions in central artery function. (submitted)
- Fleenor BS, Marshall KD, Durrant JR, Lesniewski LA, Seals DR (2010) Arterial stiffening with ageing is associated with transforming growth factor- $\beta$ 1-related changes in adventitial collagen: reversal by aerobic exercise. *J Physiol* 588.20: 3971–3982. [PubMed: 20807791]
- Fleenor BS, Seals DR, Zigler ML, Sindler AL (2012) Superoxide-lowering therapy with Tempol reverses arterial dysfunction with aging in mice. *Aging Cell* 11: 269–276. [PubMed: 22168264]
- Gleason RL, Gray SP, Wilson E, Humphrey JD (2004) A multi-axial computer-controlled organ culture and biomechanical device for mouse carotid arteries. *ASME J Biomech Engr* 126: 787–795.
- Humphrey JD (2002) *Cardiovascular Solid Mechanics: Cells, Tissues, and Organs*, Springer, NY.
- Humphrey JD (2008) Vascular adaptation and mechanical homeostasis at tissue, cellular, and sub-cellular levels. *Cell Biochem Biophys* 50: 53–78. [PubMed: 18209957]
- Humphrey JD, Eberth JF, Dye WW, Gleason RL (2009) Fundamental role of axial stress in compensatory adaptations by arteries. *J Biomech* 42: 1–8. [PubMed: 19070860]
- Humphrey JD, Dufrense E, Schwartz MA (2014) Mechanotransduction and extracellular matrix homeostasis. *Nat Rev Mol Cell Biol* 15: 802–812. [PubMed: 25355505]
- Humphrey JD, Harrison DG, Figueroa CA, Lacolley P, Laurent S (2016) Central artery stiffness in hypertension and aging. A problem with cause and consequence. *Circ Res* 118: 379–381. [PubMed: 26846637]
- Kuang SQ, Geng L, Prakash SK, Cao JM, Guo S, Villamizar C, Kwartler CS, Peters AM, Brasier AR, Milewicz DM (2013) Aortic remodeling after transverse aortic constriction in mice is attenuated with AT1 receptor blockade. *Arterioscler Thromb Vasc Biol* 33: 2172–2179. [PubMed: 23868934]
- Lacolley P, Safar ME, Regnault V, Frohlich ED (2009) Angiotensin II, mechanotransduction, and pulsatile arterial hemodynamics in hypertension. *Am J Physiol* 297: H1567–1575.
- Lakatta EG, Wang M, Najjar SS (2009) Arterial aging and subclinical arterial disease are fundamentally intertwined at macroscopic and microscopic levels. *Med Clin N Am* 93: 583–604. [PubMed: 19427493]
- Latorre M, Humphrey JD (2018) Modeling mechano-driven and immuno-mediated aortic maladaptation in hypertension. *Biomech Model Mechanobiol* (submitted).
- Laurent S, Boutouyrie P (2015) The structural factor of hypertension: Large and small artery alterations. *Circ Res* 116: 1007–1021. [PubMed: 25767286]
- Le VP, Stoka KV, Yanagisawa H, Wagenseil JE (2014) Fibulin-5 null mice with decreased arterial compliance maintain normal systolic left ventricular function, but not diastolic function during maturation. *Physiol Reports* 2: e00257.
- Lesniewski LA, Durrant JR, Connell ML, Henson GD, Black AD, Donato AJ, Seals DR (2011) Aerobic exercise reverses arterial inflammation with aging in mice. *Am J Physiol* 301: H1025–1032.
- Nilsson PM, Boutouyrie P, Cunha P, Kotsis V, Narkiewicz K, Parati G, Rietzschel E, Scuteri A, Laurent S (2013) Early vascular ageing in translation: from laboratory investigations to clinical applications in cardiovascular prevention. *J Hyperten* 31: 1517–1526
- O'Rourke MF, Hashimoto J (2007) Mechanical factors in arterial aging: A clinical perspective. *JACC* 50: 1–13. [PubMed: 17601538]
- Pezet M, Jacob MP, Escoubet B, et al. (2008) Elastin haploinsufficiency induces alternate aging processes in the aorta. *Rejuven Res* 11: 97–112.
- Ramos C, Hendgen-Cotta UB, Deenen R, Pohl J, Stock P, Hinemann C, Kelm M, Rassef T (2014) Age-related vascular gene expression profiling in mice. *Mechan Ageing Devel* 135: 15–23.
- Roccabianca S, Bellini C, Humphrey JD (2014) Computational modelling suggests good, bad and ugly roles of glycosaminoglycans in arterial mechanics and mechanobiology. *J R Soc Interface* 11: 20140397. [PubMed: 24920112]
- Roccabianca S, Figueroa CA, Tellides G, Humphrey JD (2014) Quantification of regional differences in aortic stiffness in the aging human. *J Mech Behav Biomed Matl* 29: 618–634.



- Rodriguez-Feo JA, Sluijter JP de Klein DP, Pasterkamp G (2005) Modulation of collagen turnover in cardiovascular disease. *Curr Pharm Des* 11: 2501–2514. [PubMed: 16026303]
- Safar ME (2009) Arterial aging – hemodynamic changes and therapeutic optics. *Nat Rev Cardiol* 7: 442–449.
- Sherratt MJ (2009) Tissue elasticity and the ageing elastic fibre. *Age* 31: 305–325. [PubMed: 19588272]
- Steppan J, Sikka G, Jandu S, Barodka V, Halushka MK, Flavahan NA, Belkin AM, Nyhan D, Butlin M, Avolio A, Berkowitz DE, Santhanam L (2014) Exercise, vascular stiffness, and tissue transglutaminase. *J Am Heart Assoc* 3:e000599. [PubMed: 24721796]
- Varga R, Eriksson M, Erdos MR, Olive M, Harten I, Kolodgie F, Capell BC, Cheng J, Faddah D, Perkins S, Avallone H, San H, Qu X, Ganesh S, Gordon LB, Virmani R, Wight TN, Nabel EG, Collins F (2006) Progressive vascular smooth muscle cell defects in a mouse model of Hutchinson-Gilford progeria syndrome. *PNAS* 103: 3250–3255. [PubMed: 16492728]
- Wagenseil JE, Mecham RP (2009) Vascular extracellular matrix and arterial mechanics. *Physiol Rev* 89: 957–898. [PubMed: 19584318]
- Wan W, Gleason RL (2013) Dysfunction in elastic fiber formation in fibulin-5 null mice abrogates the evolution in mechanical response of carotid arteries during maturation. *Am J Physiol* 304: H674–686.
- Weiszäcker HW, Lambert H, Pasclae K (1983) Analysis of the passive mechanical properties of rat arteries. *J Biomech* 16: 703–715. [PubMed: 6643542]
- Wheeler JB, Mukherjee R, Stroud RE, Jones JA, Ikonomidis JS (2015) Relation of murine thoracic aortic structural and cellular changes with aging to passive and active mechanical properties. *J Am Heart Assoc* 4:e001744. [PubMed: 25716945]
- Wu J, Thabet SR, Kirabo A, Trott DW, Saleh MA, Xiao L, Madhur MS, Chen W, Harrison DG (2014) Inflammation and mechanical stretch promote aortic stiffening in hypertension through activation of p38 mitogen-activated protein kinase. *Circ Res* 114: 616–625. [PubMed: 24347665]
- Zhang P, Huang A, Ferruzzi J, Mecham RP, Starcher BC, Tellides G, Humphrey JD, Giordano FJ, Niklason LE, Sessa WC (2012) Inhibition of microRNA-29 enhances elastin levels in cells haploinsufficient for elastin and bioengineered vessels – brief report. *ATVB* 32: 756–759.

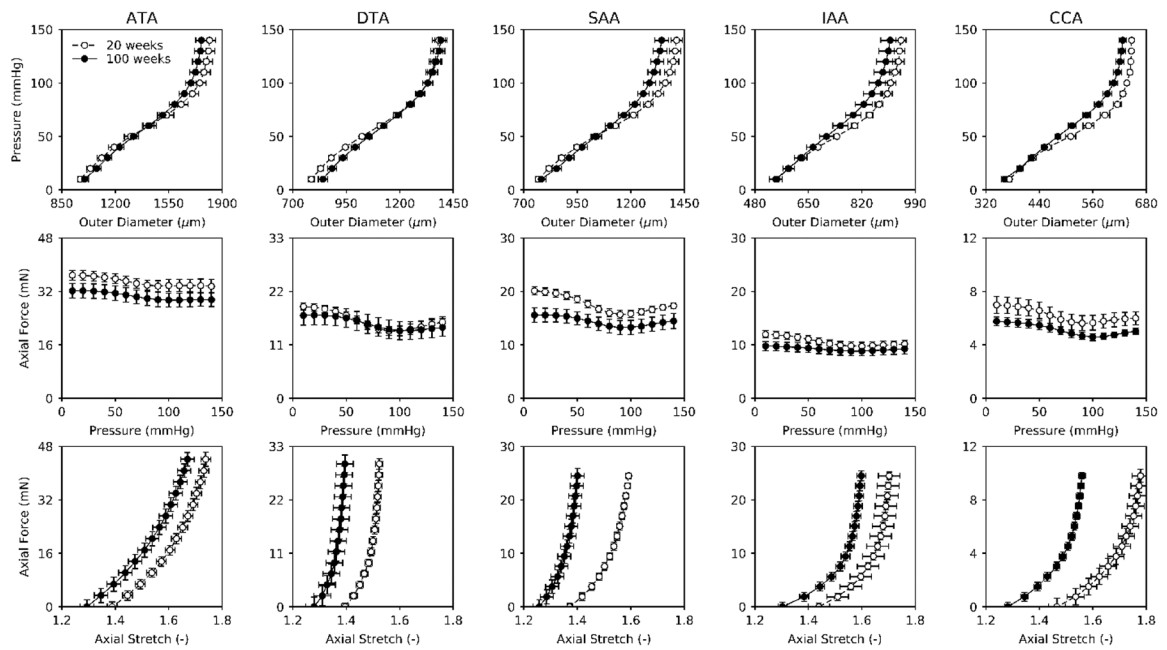


**Figure 1.**

Mean  $\pm$  SEM pressure-outer diameter ( $P-d$ ; top row) and axial force-pressure ( $F-P$ ; middle row) responses measured at individually estimated values of in vivo axial stretch plus axial force-axial stretch responses measured at a common pressure of 100 mmHg ( $F-\lambda$ ; bottom row), all as a function of murine age (20 vs. 100 weeks) and five anatomical regions: ascending thoracic aorta (ATA), descending thoracic aorta (DTA), suprarenal abdominal aorta (SAA), infrarenal abdominal aorta (IAA), and common carotid artery (CCA). Circumferential pressure-diameter behaviors are mostly unaffected by normal aging whereas axial force-stretch behaviors display a general leftward shift, which implies anisotropic structural stiffening. Note, too, the generally lower axial force needed to maintain the aged vessels at their diminished in vivo axial stretch (middle). Open circles indicate data from 20-week old mice; filled circles indicate data from 100-week old mice.

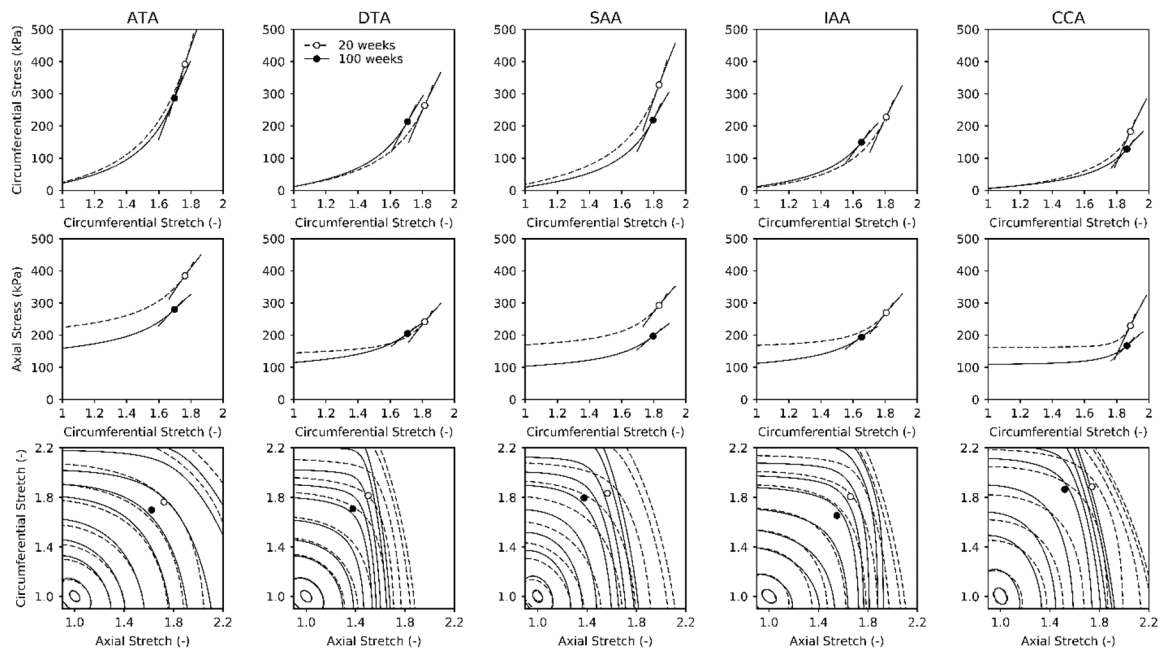


**Figure 2.** Theoretically computed Cauchy stress-stretch responses (top row, middle row), with values of linearized stiffness shown schematically by local tangents, plus the elastically stored energy shown as iso-energetic contours as a function of biaxial stretch (bottom row). The linearization was at a common distending pressure of 120 mmHg but individual axial stretches that were inferred experimentally from cross-over points in axial force – axial stretch tests. The iso-energy contours correspond to 0.1, 1, 5, 10, 20, 40, 60, 100, 250, and 500 kPa for each group, with dashed lines showing normal contours and solid lines the aged contours. Aging reduces in vivo energy levels in all regions, due in large part to the reduced in vivo axial stretches (cf. Figure 1, bottom row).

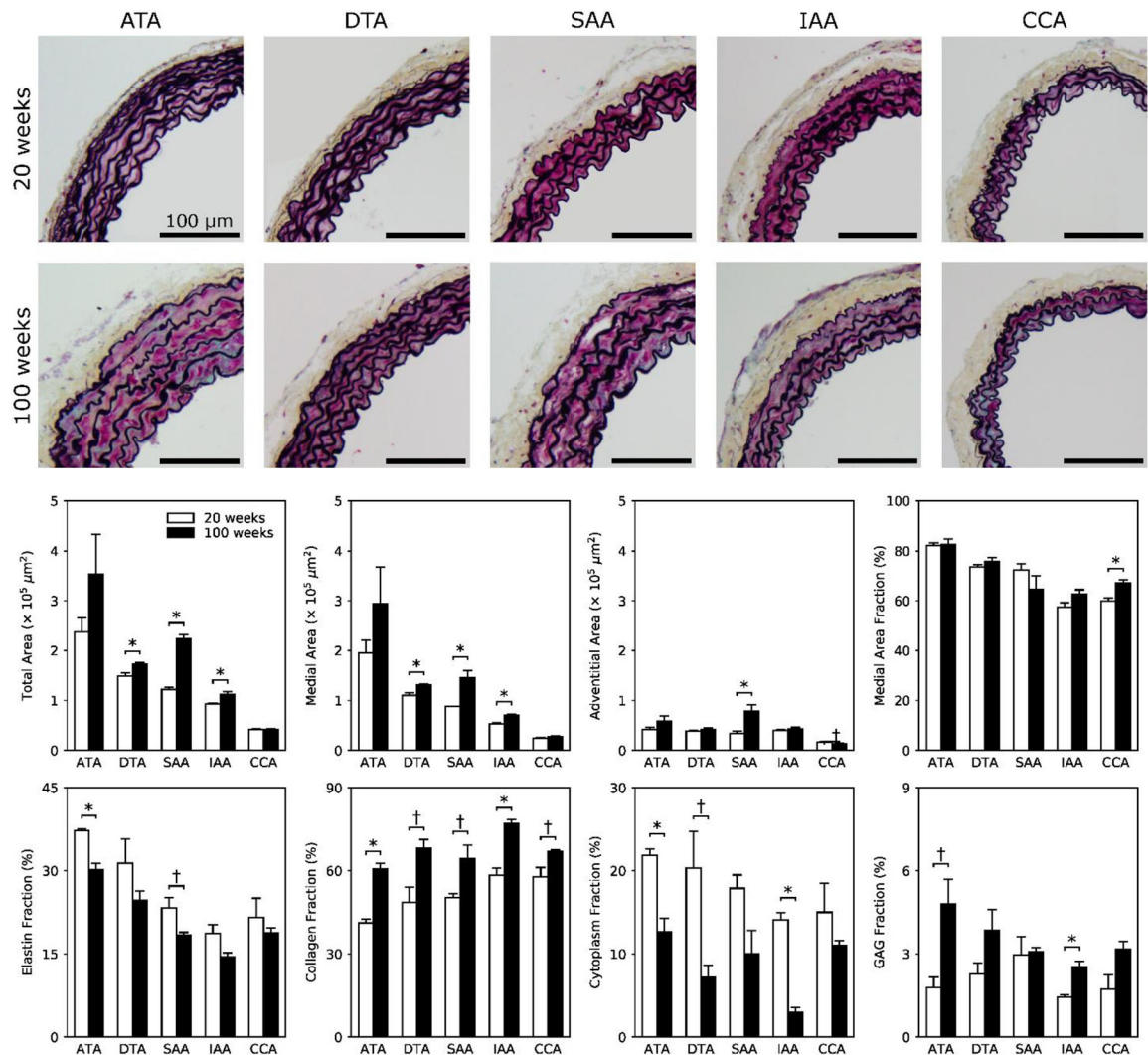


**Figure 3.** Representative bright-field Movat Pentachrome-stained images for 20-week old (first row) and 100-week old (second row) mice and each of the five regions: ATA, DTA, SAA, IAA, and CCA. Histological cross-sectional areas reflect the aging-induced thickening seen in fresh samples, but reveal further that the increase in total wall area is due mostly to an increased area of media. Shown, too, are calculated whole-wall area fractions (third row) for individual constituents (fourth row): elastin ( $\varphi^e$ ) from VVG, fibrillar collagen ( $\varphi^c$ ) and cytoplasm ( $\varphi^m$ ) from MTC, and medial glycosaminoglycans ( $\varphi^g$ ) from MOV, subject to the constraint that  $\varphi^e + \varphi^m + \varphi^c + \varphi^g \cong 1$ . The \* and † indicate significant differences, respectively, at  $p < 0.05$  and  $p < 0.10$ , between 20- and 100-week old mice.

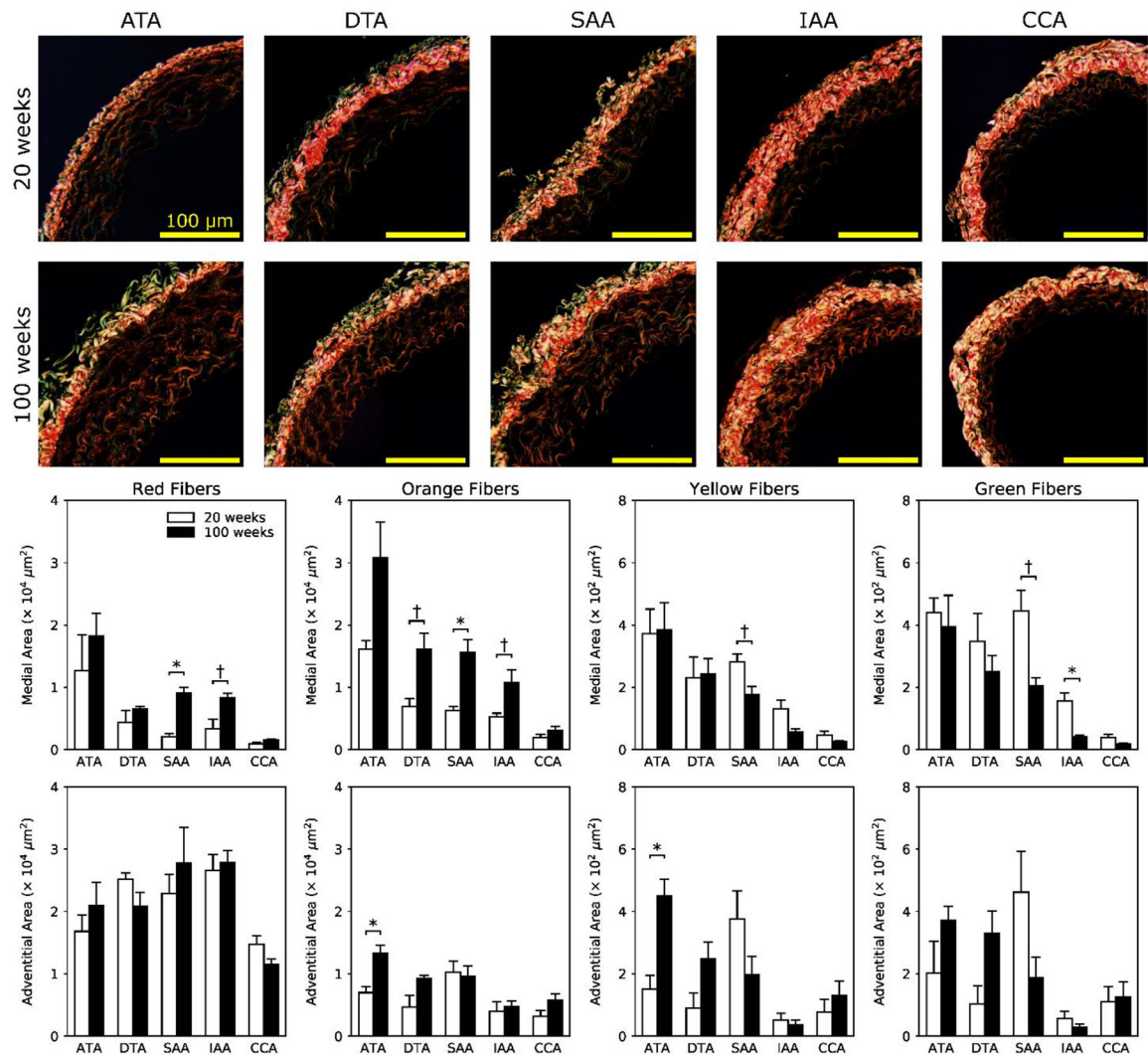


**Figure 4.** Representative dark-field picro-sirius red-stained images for 20-week old (first row) and 100-week old (second row) mice and each of the five regions: ATA, DTA, SAA, IAA, and CCA. Layer specific quantification of birefringent images (third and fourth rows) shows that normal aging associates mainly with medial remodeling of fibrillar collagen. Increased areas of thicker collagen fibrils (red-orange) and decreased areas of thinner collagen fibrils (yellow-green) are most prominent in abdominal sections (SAA and IAA). Adventitial remodeling occurred mainly in the ATA, with increased orange and yellow fibrils at 100 relative to 20 weeks of age. The \* and † indicate significant differences, respectively, at  $p < 0.05$  and  $p < 0.10$ , between 20- and 100-week old animals.

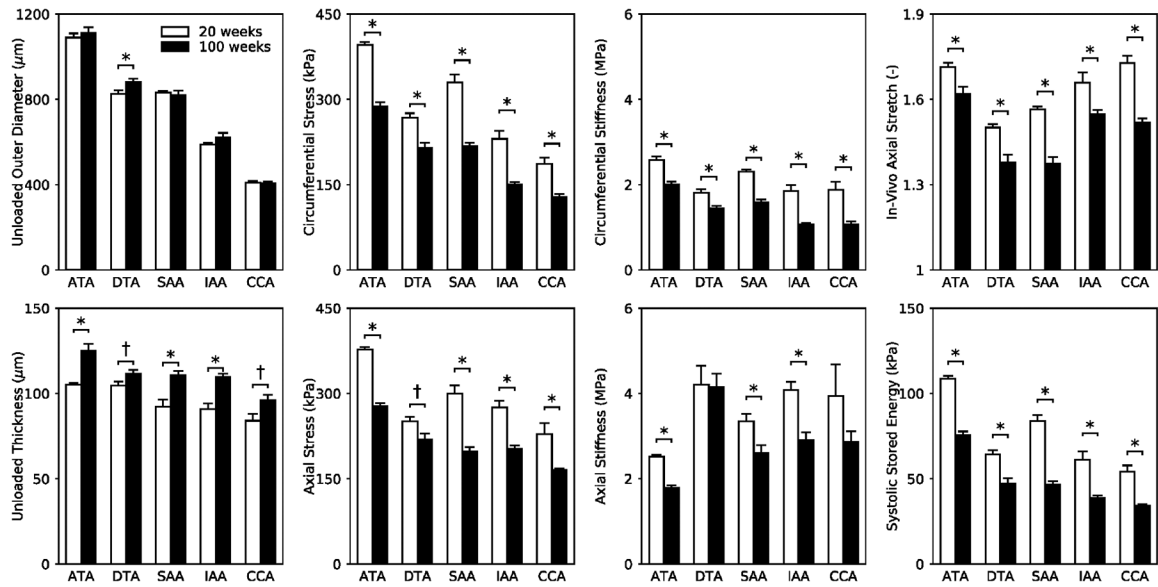


**Figure 5.** Mean  $\pm$  SEM of eight geometric or mechanical metrics (calculated at a distending pressure of 120 mmHg and individual values of in vivo axial stretches inferred from axial force-stretch tests) based on in vitro biaxial data and shown as a function of age (open bars for 20-week old and filled bars for 100-week old vessels) and five anatomical regions: ATA, DTA, SAA, IAA, and CCA. Importantly, the increased unloaded wall thickness and decreased in vivo axial stretch in each region contribute to the nearly uniform decrease in elastic energy storage, biaxial Cauchy stress, and biaxial material stiffness. The \* and † indicate significant differences, respectively, at  $p < 0.05$  and  $p < 0.10$ , between 20- and 100-week old animals. See Table S1 for corresponding values.

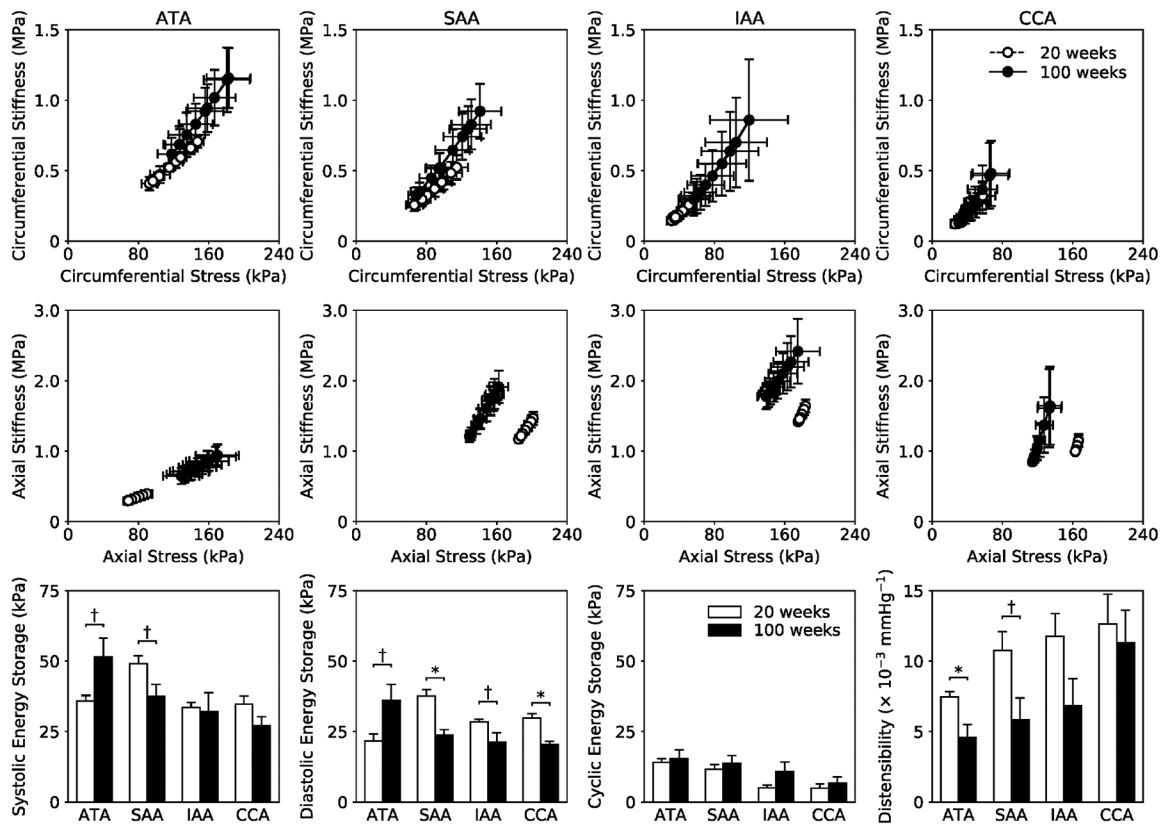


**Figure 6.**

Biaxial material stiffness-stretch behaviors (top, middle rows) calculated for in vivo conditions by combining material properties quantified in vitro with motions measured in vivo using ultrasound. Circumferential properties (top row) are preserved while axial properties (middle row) are altered with aging. In vivo energy storage  $W$  and distensibility  $D$  (bottom row) are altered primarily in the ATA and SAA, with diastolic energy storage also showing differences in the IAA and CCA. Cyclic energy storage, which characterizes the in vivo capacity to store elastic energy at systole for use during diastole to work on the blood or heart, is remarkably unaffected by aging under anesthetized conditions. Note, too, that increased energy storage, wall stress, and material stiffness in the ATA appear to have resulted from its lengthening with aging. In contrast, the SAA, IAA, and CCA show a general trend of decreased energy storage and Cauchy stress with preserved stiffness. The \* and † indicate significant differences, respectively, at  $p < 0.05$  and  $p < 0.10$ , between 20- and 100-week old animals.

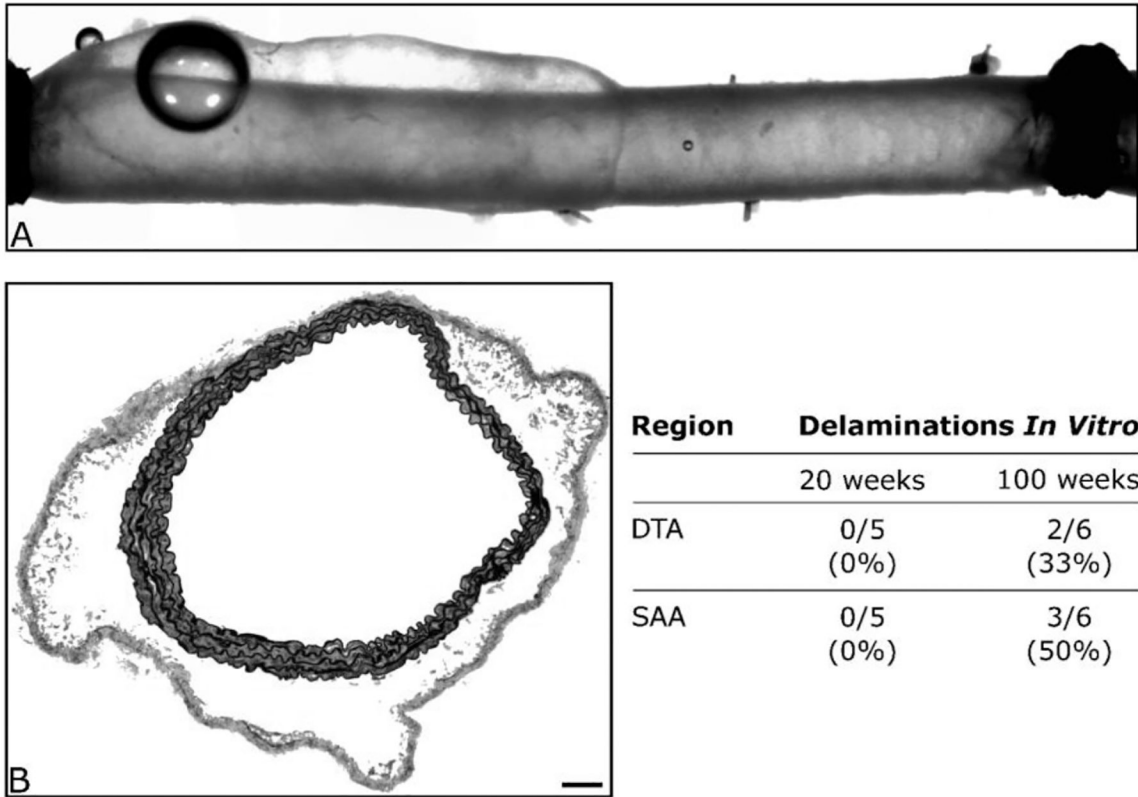


**Figure 7.** Shown are an illustrative (panel A) video-capture during standard biaxial testing of a DTA that was excised from a 100-week old mouse and (panel B) histological image of a SAA following mechanical testing. Both images reveal a propensity to develop an intramural delamination without frank rupture. Such delaminations consistently occurred at the medial-adventitial border and appeared to initiate at or near branches. The scale bar represents 100  $\mu\text{m}$  in panel B.



**Table 1.**

Baseline transthoracic ultrasound measurements of cardiac function for 20-week and 100-week old male wild-type mice. Systolic function (top portion) is mostly preserved while measurements of left ventricular (LV) volume and mass show that normal aging associates with LV hypertrophy. Diastolic function (bottom portion) is diminished in the older mice as revealed by a decreased E/A ratio, mostly due to an increased velocity of atrial filling (A peak).

	20 weeks	100 weeks
n	5	6
Heart Rate (bpm)	409 ± 29	434 ± 20
Diastolic Thickness (mm)		
IVS	0.89 ± 0.06	1.08 ± 0.05*
LW	0.81 ± 0.08	1.05 ± 0.06*
Internal Diameter (mm)		
Diastolic	3.92 ± 0.21	4.22 ± 0.14
Systolic	2.55 ± 0.16	2.87 ± 0.15
Volume (µL)		
Diastolic	68 ± 9	81 ± 6
Systolic	24 ± 4	33 ± 4
SV (µL)	44 ± 5	48 ± 3
CO (mL/min)	17 ± 1	21 ± 2
EF (%)	65 ± 1	60 ± 3
FS (%)	35 ± 1	32 ± 2
LV Mass (mg)	127 ± 22	190 ± 9*
LV/Body Mass (mg/g)	4.2 ± 0.1	6.4 ± 0.3*
Filling Velocity (mm/s)		
E Peak	684 ± 87	655 ± 51
A Peak	473 ± 65	628 ± 72
E/A Ratio	1.45 ± 0.03	1.04 ± 0.12*
DT (ms)	29.8 ± 1.6	32.3 ± 0.8
IVS Velocity Ratios		
A'/E'	1.34 ± 0.22	1.44 ± 0.12
E'/A'	0.84 ± 0.20	0.71 ± 0.06
LW Velocity Ratios		
A'/E'	1.34 ± 0.07	1.46 ± 0.06
E'/A'	0.75 ± 0.04	0.69 ± 0.03

The \* indicates significant differences, at  $p < 0.05$ , between 20- and 100-week old animals.

IVS – interventricular septum; LW – lateral (LV) wall; SV – stroke volume; CO – cardiac output; EF – ejection fraction; E and A – ventricular filling velocity in early (E) and late (A, due to atrial contraction) diastole measured with Doppler; E' and A' – similar, but based on tissue Doppler. DT – deceleration time is the time taken from the maximum E to baseline.